

**Jet-Mixing for the Production of Monodisperse Silver Nanoparticles Using Reduced Amounts of Capping Agent**

Journal:	<i>Reaction Chemistry & Engineering</i>
Manuscript ID	RE-ART-04-2019-000152
Article Type:	Paper
Date Submitted by the Author:	08-Apr-2019
Complete List of Authors:	Ranadive, Pinaki; Ohio State University, Chemical and Biomolecular Engineer Parulkar, Aamena; Ohio State University, Chemical and Biomolecular Engineering Brunelli, Nick; Ohio State University, Chemical and Biomolecular Engineer

27 1. Introduction

28 Important materials discoveries continue to emerge as the ability to generate nanomaterials with
29 exquisite control on the lab scale advances. However, translating these exciting discoveries into commercial
30 processes offers considerable challenge, especially because of the difficulties associated with scalability of
31 small-scale synthetic techniques. Indeed, many of these nanomaterials are synthesized in small scale batch
32 processes that allow precise control over many important synthetic conditions, including reaction
33 temperature, mixture composition, and other parameters that can affect the final size distribution and even
34 the morphology of the nanoparticles (NPs) formed.¹ The mixing dynamics in the reaction system directly
35 influence the ability to control these parameters. For small scale synthesis, it is possible to control these
36 different parameters sufficiently to produce nanomaterials with a monodisperse particle size distribution
37 (PSD). However, scaling up these syntheses to produce larger quantities of nanomaterials often results in
38 complications since controlling synthetic parameters for batch methods when operating at larger length
39 scales is difficult.² Thus, it remains a challenge to develop methods for the scalable manufacturing of
40 nanoparticles with the same quality as achieved in small-scale synthesis.

41 The synthesis of nanomaterials is commonly accomplished using liquid-phase methods. Since
42 liquid-phase methods are broadly applicable to many materials,³ advances in nanomaterial synthesis can be
43 achieved through investigating a single material. A convenient system to investigate is the production of
44 silver nanoparticles. Silver nanoparticles have many applications, including as biosensing and bio-imaging
45 agents,^{4,5} catalysts in several reactions, and anti-microbial additives.^{5,6} Silver nanoparticles are a convenient
46 system to investigate since they exhibit localized surface plasmon resonance (SPR), in which the interaction
47 of light with the electrons in the conduction band of an Ag particle results in a specific resonant oscillation.⁷
48 The frequency of this oscillation provides information about several properties of the NP colloid, including
49 particle size and shape.^{8,9} The frequency falls into the visible range of the electromagnetic spectrum for
50 nanomaterial systems such as Ag and Au, and hence can be characterized by UV-vis spectroscopy.
51 Interestingly, the extent of broadness of the SPR spectrum, measured by its full width at half maximum

52 (FWHM), is indicative of the polydispersity of the sample.¹⁰ Generally, a broader PSD will have a larger
53 FWHM in the UV-vis spectrum.

54 Typically, these metal nanoparticles are synthesized by the injection of a reducing agent into a
55 solution containing a nanoparticle precursor to induce nanoparticle nucleation and growth.³ Each of the
56 components in the mixture needs to be balanced carefully since the concentration of each can impact the
57 final product properties, including the particle size and the PSD. Controlling the PSD is often important
58 since the NP performance is often a function of size. Although not all applications require monodisperse
59 PSDs,¹¹ most applications benefit from having monodisperse particle sizes. For example, a recent study
60 demonstrated that large Ag nanoclusters were more selective for the partial oxidation of propylene.¹² In
61 addition to the performance of NP, a uniform PSD can also affect the stability of NP solutions. A
62 monodisperse PSD tends to increase the colloidal stability of the distribution post-synthesis according to
63 derivations of the classical nucleation theory (CNT), limiting particle growth phenomena such as Ostwald
64 ripening.³ This can be important as the colloidal stability can affect the shelf life for these materials.

65 Synthesizing NPs with a well-characterized and stable PSD can be challenging since the PSD can
66 broaden either during or after the synthesis, making it necessary to prevent aggregation and Ostwald
67 ripening from altering the PSD. Two common methods to control PSD are using reverse micelles and using
68 capping agents.¹³⁻¹⁶ Reverse micelles utilize surfactants to produce a bi-phasic system consisting
69 predominantly of an organic phase with dispersed droplets of an aqueous phase containing the reactants.
70 The organic medium between micelles isolates NPs, preventing agglomeration¹⁵ and allowing control over
71 the final particle size.¹⁶ However, the requirement of an organic solvent makes reverse micelles biologically
72 and environmentally less friendly. In contrast, nanoparticle synthesis can be accomplished in a single phase
73 through utilizing capping agents. Capping agents are ionic species or bulky molecules that provide an
74 electrostatic or steric barrier, respectively, between individual NPs in solution to prevent agglomeration.
75 This method is a preferred choice in toxicity studies¹⁷ and is also used by commercial vendors.^{12,13}

76 The beneficial aspects of utilizing a capping agent needs to be balanced with the cost of the capping
77 agent when considering the scalable manufacture of nanomaterials. From an economic perspective, the

78 amount of capping agent utilized should be the minimum that can produce the desired product quality. From
79 a scientific perspective, the concentration of the capping agent plays an important role in determining NP
80 stability. At too low of a capping agent concentration, the surface of the NPs is not sufficiently “capped”
81 and aggregation takes place because of van der Waals attraction. Interestingly, it can be problematic to use
82 an excessive amount of capping agent since many common capping agents like trisodium citrate (TSC) are
83 ionic. At high concentrations, the capping agent can dissociate in solution, increasing the ion concentration
84 of the solution. According to the DLVO theory, high ion concentration can lower the electrostatic barrier
85 between two particles, promoting aggregation.^{18,19} Hence, it is hypothesized that there is a “just right”²⁰
86 concentration of capping agent at which NPs may remain stable. At this intermediate concentration, steric
87 or electrostatic repulsion prevents aggregation, leading to stable colloidal nanoparticles in solution. Besides
88 affecting NP stability, capping agents remaining in solution can also have other undesired effects such as
89 altering the particle morphology^{1,21} or hindering catalytic activity.²² Most importantly, considering the
90 holistic goal of scaling up NP syntheses, reducing the amount of capping agent used can reduce the overall
91 process cost. Hence, it is desirable to optimize the amount of capping agent used for synthesizing a
92 monodisperse PSD. Current synthetic methods report utilization of capping agent concentrations that are
93 equal to or higher than the concentration of metal precursor in solution.^{10,13,16–22} It is unclear if this
94 concentration represents an optimum for the synthesis or is the concentration required for batch processes
95 to maintain a narrow PSD.

96 In addition to using an optimal amount of capping agent, a narrow PSD requires creating uniform
97 reaction conditions to enable uniform nucleation and growth. Uniform conditions can be generated through
98 inducing intense mixing to reduce the timescale for mixing (τ_{mix}) below the timescale for reaction ($\tau_{reaction}$).
99 For solution-phase Ag NP synthesis, the process involves the reduction of Ag^+ ions to Ag^0 atoms that
100 nucleate and grow to form NPs. The reduction is commonly achieved through using a reducing agent³³ such
101 as $NaBH_4$ ^{34–37} that is highly active and reacts on the timescale of milliseconds.³⁸ This rapid reaction time
102 makes it necessary to create intense mixing so that uniform reaction conditions can be obtained. When

103 scaling up the batch process, it is challenging to generate the intense mixing necessary to produce a narrow
104 PSD, often resulting in batch-to-batch variability.^{39,40}

105 Efficient mixing requires controlling the process at all spatial scales, including macromixing,
106 mesomixing, and micromixing.⁴¹ Macromixing refers to achieving composition homogeneity within the
107 bulk of the fluid, mesomixing occurs at the different scales of eddies in the fluid, and micromixing at the
108 molecular level between fluid lamellae. Each spatial scale has an associated time-scale that add in series to
109 comprise the overall τ_{mix} . In a batch reactor, the volume is large enough that the overall mixing process can
110 be limited by macromixing.² Poor macromixing for batch reactors can cause non-uniformity in the reactant
111 concentrations and temperature throughout the volume of the batch. Hence, fast reactions such as redox or
112 neutralization reactions, progress with different rates spatially in the reactor,⁴² resulting in a wide PSD for
113 NP synthesis solutions. From previous work for colloidal syntheses, a direct link exists between τ_{mix} and
114 the PSD of the NPs synthesized.⁴³ The importance of macromixing can be mitigated through reducing the
115 dimensions of the reactor as is possible in microfluidic and millifluidic devices.⁴⁴ Microfluidic technologies
116 for nanoparticle synthesis take advantage of the small τ_{mix} that is a result of their compact volume.^{45,46} While
117 continuous flow microfluidic devices can obviate macromixing, it is still important to achieve efficient
118 mesomixing and micromixing when using highly active reducing agents.

119 Several continuous syntheses at both ambient conditions and high temperatures, and in gas and
120 liquid phase, have been explored for Ag NPs.^{28,32,47-55} Two notable geometries are a coaxial mixing system
121 and an impinging jet reactor. The coaxial mixing system used high flow rates to increase mixing and
122 produce nanoparticles⁴⁸ that would be promising if issues with radial mixing can be overcome. Impinging
123 jet reactor was able to prevent clogging, but the size distribution obtained by the continuous process was
124 broad.⁴⁹ Continuous flow synthesis of nanomaterials would be promising if the reactor could achieve better
125 mixing dynamics. Another reactor type, the segmented flow reactor is known to offer a narrow size
126 distribution because of minimized axial dispersion, but liquid cross-mixing between individual segments
127 because of menisci on the walls may actually broaden the PSD.^{52,56} Recently, our research group

128 demonstrated the continuous synthesis of zeolitic imidazolate frameworks (ZIFs) using a continuous jet-
129 mixing reactor.⁵⁷ The jet-mixing reactor enabled efficient mixing for the rapid nucleation and growth of
130 ZIFs, resulting in narrow PSD that caused the ZIFs to be stable colloidal suspensions. The jet-mixing reactor
131 also had a small reactor volume that efficiently synthesized the nanomaterials with high yields and high
132 productivities.

133 In this work, the jet-mixing reactor is used to synthesize Ag NPs in a continuous manner. The
134 nanoparticles are analyzed using common characterization methods, including transmission electron
135 microscopy (TEM), Ultraviolet-visible absorption (UV-vis) spectroscopy, and dynamic light scattering
136 (DLS). The properties of Ag NPs obtained by batch synthesis are compared to those obtained by jet-mixing
137 synthesis. Both the batch and jet-mixing synthesis are examined for batch-to-batch variability. For the jet-
138 mixing reactor, the effect of the flow rate, the concentration of the reducing agent, and the capping agent
139 on the PSD of Ag NPs is examined. With jet-mixing reactor, a reduced capping agent concentration is found
140 to be sufficient to stabilize the nanoparticles. To understand the stabilization, experiments are conducted to
141 study the effect of the ion concentration of the solution. Overall, this work demonstrates that the jet-mixing
142 reactor is a promising continuous system for the synthesis of silver nanoparticles.

143 2. Experimental Methods

144 2.1. Chemicals

145 All chemicals are used as received without further purification, including: silver nitrate (AgNO_3 ;
146 >99%, ACS grade; VWR Life Science), trisodium citrate dihydrate (TSC; > 99%, ACS grade, BDH
147 Chemicals), sodium nitrate (NaNO_3 ; 98% Beantown Chemical), and sodium borohydride (NaBH_4) solution
148 (12 wt%) in 14 M NaOH (Sigma Aldrich). All solutions are prepared using deionized (DI) water.

149 2.2. Reactor design

150 The design of the reactor has been adapted from a gas-phase synthesis⁵⁸ and has been used by our
151 group for successful ZIF-8 synthesis in liquid phase.⁵⁷ The reactor design and assembly are shown in Figure
152 1. The reactor is manufactured in-house from a thermally and chemically resistant polyether ether ketone
153 (PEEK) cube (1" x 1" x 1"). The cube consists of three cylindrical flow channels (one main line and two

154 jets) that intersect in a perpendicular manner in the center of the device. A flow channel with diameter
155 (d_{main}) of 0.04 inch (1.02 mm) goes through the entire length of the reactor and is called the main line. Two
156 identical jet lines with a diameter (d_{jet}) of 0.02 inch (0.51 mm) impinge perpendicularly at the center of
157 device with the main line. Although the jets impinge from opposite sides of the main line, both jet lines are
158 drilled starting from one side of the cube to ensure that the jet lines are properly aligned, as has been done
159 for confined impinging jet reactors.⁴¹ The channels are threaded at the ends to enable connection of clear
160 polytetrafluoroethylene (PTFE, ID 0.03") tubing using appropriate microfluidic PEEK fittings. The main
161 line delivers the reducing agent solution while the jet-line delivers the silver substrate and capping agent
162 solution. The reactants are pumped using two KD Scientific 100KD syringe pumps. For the jet lines, a Y-
163 adapter is used to split the flow from the syringe pump into two streams, each of which connects to one of
164 the jets. From control experiments, it has been determined that Ag NP synthesis is insensitive to differences
165 in flow between the two jets (Section 5). The combined jet lines and main line flows comprise the product
166 solution that flows out downstream of the reactor. The outlet product stream is collected in a flask covered
167 with aluminum foil and stored in an ice bath.

168 2.3. *Batch synthesis of silver nanoparticles (Ag NPs)*

169 Initial studies involve comparing Ag NPs synthesized using concentrations utilized for batch
170 methods reported previously.^{36,59} For the Ag NP synthesis, an aqueous solution of 0.2 mM AgNO₃ and 0.2
171 mM TSC is prepared at room temperature. An equal volume of aqueous solution of 0.6 mM NaBH₄ is
172 prepared. The NaBH₄ solution is prepared in an ice bath and cooled for 20 minutes before use. All batch
173 experiments are carried out in a 250 mL round-bottom flask. In a standard batch synthesis, 50 mL of the
174 NaBH₄ (0.6 mM) solution that has been cooled is placed in the 250 mL flask and stirred at 200 RPM using
175 a PTFE-coated stir bar. To this solution is added the AgNO₃ and TSC solution (50 mL). As previous
176 literature reports, stirring is stopped after 2 minutes and the solution is stored in the refrigerator at 4-6°C.^{16,60}
177 Further details on the synthesis procedure can be found in the supplementary information (Section 1). A
178 different order of reagent addition involving the addition of the NaBH₄ solution to the AgNO₃ and TSC

179 solution in batch, was also tested. Both methods produce comparable nanoparticles, as suggested by the
180 UV-vis spectra in Figure S14.

181 2.4. *Flow synthesis of silver nanoparticles using a jet-mixing reactor*

182 The standard jet-mixing synthesis is performed using a solution with concentrations of 0.2 mM
183 AgNO₃ and 0.2 mM TSC in water and a separate solution with 0.6 mM NaBH₄ in water. The solutions are
184 loaded into separate syringes. The syringe with NaBH₄ is connected to the main line and the silver salt and
185 TSC solution is connected to the jet line. For the standard experiment, the syringe pumps are set to a flow
186 rate of 48 mL/h. These are the flow rates that are determined to provide sufficiently intense mixing to
187 produce a monodisperse PSD, as shown in the supplementary information in Figure S1. The experiment to
188 find these flowrates is described in the SI (Section 2). The beaker in which the jet-mixing product is
189 collected is placed in an ice bath. The collection beaker in jet-mixing or the round-bottom flask in batch are
190 both covered with aluminum foil to limit photolytic reduction of AgNO₃.⁶⁰ Further details on the synthesis
191 procedure can be found in the SI (Section 1.1 and 1.3).

192 2.5. *Material characterization*

193 All analyses are performed within one hour of synthesis. The product Ag NP solution is
194 characterized primarily via UV-vis, DLS, and TEM. UV-vis analysis is performed using a ThermoFisher
195 Evolution 300 UV-vis spectrophotometer with a Xenon lamp using a bandwidth of 2 nm and a scan speed
196 of 600 nm/min. After the particles have been synthesized, the product solution (1 mL) is diluted with DI
197 water (1 mL) in a 1 cm pathlength quartz cuvette. Fifteen minutes after synthesis, the UV-vis spectrum for
198 the sample is recorded. The data are analyzed through fitting the data to determine the wavelength
199 maximum (λ_{max}) and the full width at half maximum (FWHM) of the UV-vis spectrum, as described in the
200 supplementary information (Section 3). The PSD is also investigated using DLS analysis using a
201 Brookhaven Instruments Corporation BI-200SM Goniometer. The sample (1 mL) is filtered using a 0.2 μ m
202 PTFE syringe filter before DLS is performed using a 637 nm laser beam at a detector angle of 90° with a
203 dust cut-off of 20 μ m. The solvent is set as water and the temperature at 20°C. Three runs are conducted
204 for each sample with the average being recorded to calculate the PSD. Analysis is done via the Brookhaven

205 Instruments Dynamic Light Scattering software. For most samples, the PSD is corroborated through using
 206 a FEI Tecnai G2 Spirit TEM at a voltage of 80 kV and magnification of 115,000x in bright-field mode.
 207 TEM samples are prepared on 150 mesh holey-carbon copper grids by dropping 15 μL of sample on the
 208 grid 1 hour after collection and letting dry for up to 2 hours in a partially covered Petri dish to prevent
 209 contamination. Particle size analysis is performed using ImageJ software.⁶¹ More information about the
 210 analysis is included in the supplementary information (Section 3).

211 3. Results and Discussion

212 3.1. Theoretical comparison of the mixing time scales in the batch and jet-mixing reactor

213 The mixing time (τ_{mix}) can be estimated for an idealized turbulent mixer as:

$$214 \quad \tau_{\text{mix}} = 3.3 \left(\frac{ML^2}{P} \right)^{\frac{1}{3}} \quad (1)$$

215 Where, M is the mass of fluid in the dissipation region, L is the characteristic length of the dissipation
 216 region, and P is the mechanical power introduced into dissipation volume. The power input into the system
 217 is the total kinetic energy of the incoming main line (diameter, $d_{\text{main}} = 0.04''$) stream with flowrate Q_0
 218 and velocity v_0 , and the incoming jet line (diameter, $d_{\text{jet}} = 0.02''$) stream with total flowrate Q_1 and
 219 velocity v_1 . Hence, P can be expressed as:

$$220 \quad P = \sum \rho v_i^2 Q_i \quad (2)$$

221 L can be estimated as the diameter of the jet line. Combining these into (1), τ_{mix} can be expressed as:

$$222 \quad \tau_{\text{mix}} = 3.3 \left(\frac{\frac{1}{32} \pi^2 d_{\text{main}}^2 d_{\text{jet}}^3}{\frac{Q_0^3}{d_{\text{main}}^4} + \frac{4Q_1^3}{d_{\text{jet}}^4}} \right)^{\frac{1}{3}} \quad (3)$$

223 For the standard flowrates ($Q_0 = Q_1 = 48 \text{ mL/h}$) used for synthesis, the estimated τ_{mix} is 22 ms.

224 In comparison, it has been estimated that for a 250 mL cylindrical flask (diameter = 55 mm), the time for
 225 95% mixing of a water-like fluid with a 2.5 cm magnetic stir-bar at 500 RPM, is $\tau_{\text{mix}} = (8.3 \pm 1.4) \text{ s}$. This

226 suggests that for Ag NP synthesis, the τ_{mix} for the batch reactor is over two orders-of-magnitude slower than
227 for the jet-mixing reactor operating at standard conditions.

228 Experimentally, it is found that increasing the mixing time in the jet-mixing reactor by operating at
229 a main line and jet line flowrate of 2 mL/h with standard reagent concentrations results in an Ag NP sample
230 that has a UV-Vis spectrum with its FWHM approaching that of a standard Ag NP batch, suggesting that
231 the mixing time plays an important role in Ag NP monodispersity. The plot comparing the UV-Vis spectra
232 for the jet-mixing sample at 2 mL/h and the standard batch sample is shown in Figure S1.

233 3.2. Standard batch and jet-mixing synthesis

234 Initial work with the jet-mixing reactor demonstrates the successful synthesis of Ag NPs using the
235 standard concentrations of 0.2 mM AgNO₃, 0.2 mM TSC, and 0.6 mM NaBH₄. The silver nanoparticles
236 produced in the jet-mixing reactor are characterized by UV-vis, TEM imaging, and DLS. As can be
237 observed in Figure 2, the UV-vis spectrum has a single sharp peak that is consistent with a narrow PSD.
238 The spectrum can be fit to obtain both the absorbance maximum (λ_{max}) and the full-width at half-maximum
239 (FWHM). For the standard conditions with the jet-mixing reactor, the particles are found to have a $\lambda_{\text{max}} =$
240 389 nm and a FWHM = 57 nm, which is consistent with a monodisperse PSD.

241 The actual PSD for this synthesis is investigated using TEM to corroborate the UV-vis spectrum.
242 Several images (Figure 3a shows a representative TEM image; additional images are shown in Figures S5)
243 are taken from different locations on the TEM grid, with over 300 particles being used for PSD analysis.
244 Using ImageJ software,⁶¹ it is determined that the jet-mixing reactor produces a monodisperse distribution
245 with a mean particle size of 5±2 nm. The particle size measured with TEM is consistent with the UV-vis
246 spectrum. While TEM imaging is useful to directly visualize particles, TEM sample preparation and
247 analysis are resource intensive, making it desirable to characterize the PSD with alternative methods such
248 as DLS. Analyzing the jet-mixing synthesis with DLS reveals a PSD of 7±2 nm. As DLS measures the
249 hydrodynamic diameter of the particle, it is expected to be greater than the size obtained by TEM. While
250 the size measured via DLS is only slightly greater than that obtained via TEM, the close match suggests

251 that the combination of UV-vis and DLS can be used to characterize the silver nanoparticles with TEM
252 providing corroborating evidence. The DLS data are shown in Figure S6 and Table S2.

253 For comparison, the standard synthesis concentrations are used in a batch process and result in the
254 formation of nanoparticles. These are characterized using UV-vis (Figure 2), TEM (Figure 3b), and DLS
255 (Figure S6 and Table S2). The UV-vis spectrum is shown in Figure 2. Similar to the jet-mixing sample, the
256 UV-vis spectrum has a prominent surface plasmon resonance (SPR) peak, confirming the synthesis of Ag
257 NPs. While the UV-vis spectrum has a sharp peak at a $\lambda_{max} = 389$ nm, it also has a shoulder at 410 nm.
258 Since it is generally established that a longer wavelength of absorption corresponds to a larger particle size²⁹
259 or a non-spherical morphology,²³ the shoulder in the UV-vis spectrum suggests the coalescence of particles.
260 Comparing the nanoparticles made with the batch and the jet-mixing, the two spectra have similar
261 intensities, but the batch synthesis results in a bimodal distribution with a broader UV-vis spectrum. These
262 batch samples are also investigated with TEM to determine the PSD, as shown in Figure 3b. From
263 multiple TEM images, the PSD calculated from analyzing over 300 particles is found to be 9 ± 4
264 nm. Consistent with the UV-vis data, this PSD appears to have a primary particle population
265 around 8 nm and an extended tail of larger particles between 16 nm. In addition to Figure 3b, other
266 TEM images used for PSD calculation using ImageJ are shown in Figure S7. The PSD from DLS
267 is 13 ± 3 nm, which is comparable with the PSD determined from TEM images. The DLS data are
268 shown in Figure S6 and Table S2.

269 In comparison to batch synthesis, the jet-mixing reactor produces a more uniform PSD, as is
270 evidenced by comparing the size distribution obtained from TEM. This observation indicates the τ_{mix} is
271 important consideration for Ag NPs. It is thought that a secondary stage of particle formation avoided by
272 using jet-mixing in comparison to batch, as indicated by the UV-vis spectra of the samples produced using
273 the two methods. Further, it is observed that the jet-mixing synthesis produces a smaller mean particle size
274 than the batch process. This is attributed to the efficient micromixing in the jet-mixing reactor that creates
275 uniform nucleation conditions that induces a higher rate of nucleation. Since the total available silver

276 substrate is limited, the formation of a greater number of nuclei results in the growth of the nuclei being
277 stoichiometrically limited. This observation of a smaller particle size being produced via microreactor
278 synthesis as compared to batch, has been reported for other microfluidic Ag NP syntheses.^{37,62} The obtained
279 sizes for the batch and jet-mixing synthesis are in agreement with those previously reported in
280 literature.^{37,48,49,62–64} NaBH₄ being among the more active reducing agents typically results in faster reaction
281 kinetics, leading to rapid nucleation and a small particle size (<10 nm). Among the microfluidic syntheses
282 with a mean size of 3 – 5 nm, the standard deviation obtained varies between 30 – 50%. The PSD obtained
283 from the jet-mixing reactor for standard operating conditions falls within this range.

284 Along with monodispersity, another important consideration for the synthesized Ag NPs is particle
285 yield. The absorbance associated with the SPR peak of the Ag NPs, obtained from the UV-vis spectrum,
286 can be correlated with NP concentration using Beer's law.²⁹ Using this method, the yield for the batch and
287 jet-mixing synthesis is calculated to be 88% and 82% respectively, suggesting that the material efficiency
288 of the two processes is comparable. The detailed calculation of yield is outlined in the supplementary
289 information in Section 4.

290 **3.3. Reproducibility tests for the jet-mixing synthesis**

291 One of the main advantages of a flow synthesis over a batch synthesis is the potential to achieve
292 greater reproducibility in the synthesis conditions (i.e., mixing) to eliminate batch-to-batch variability.
293 Specifically, it is desirable to demonstrate that the reactor performs (1) stably over a single continuous test
294 and (2) consistently across different tests. For Ag NPs, UV-vis is a facile method to test variability between
295 properties across different samples by comparing the λ_{max} and FWHM of the SPR absorbance peak.

296 Initially, the continuous steady-state operation of the jet-mixing reactor is tested by checking the
297 variability within a single continuous run. The UV-vis spectra from a standard jet-mixing Ag NP synthesis
298 over its run-time (i.e., start of the synthesis to end of the synthesis) are monitored, to ensure that the Ag
299 NPs synthesized in a continuous run have similar properties at different sampling times. The product
300 solution from an hour-long run is collected intermittently every 15 minutes and analyzed by UV-vis after

301 collection. The absorbance, λ_{max} and FWHM are noted for each sample. The UV-vis spectra overlap for
302 each sample collected (samples S1 to S5) shown in Figure 4, indicating that Ag NPs with similar properties
303 are formed at all times. Quantitatively, the standard deviation of the properties of the UV-vis spectra
304 between the various samples is <5%, corroborating the uniformity in Ag NP properties. The data are
305 reported in Table S3.

306 Next, multiple batch and jet-mixing runs with the standard reagent concentrations are conducted to
307 compare the variability across the runs for the two synthesis methods using the standard conditions for each
308 method. Each synthesis is analyzed by UV-vis. It is observed that for batch synthesis, the UV-vis spectra
309 vary from batch to batch despite efforts to maintain all synthesis parameters constant. This is qualitatively
310 indicated by Figure 5a for four different runs attempted using identical conditions. Quantitatively, the
311 variability between batches is greater than 5% for the FWHM and the intensity of the UV-vis spectrum, as
312 indicated by the standard deviation of the parameters for all runs. The quantitative variability in these
313 parameters is provided in Table S4. A similar experiment with the jet-mixing reactor shows lesser
314 variability between four identical runs, as is qualitatively shown in Figure 5b, demonstrating its ability to
315 produce Ag NPs with consistent properties over multiple separate runs. The quantitative variability in these
316 parameters is provided in Table S5. It is hence concluded that jet-mixing results in more reproducible
317 synthesis of Ag NPs with monodisperse narrow PSD as compared to batch synthesis.

318 **3.4. Effect of synthesis parameters in jet-mixing synthesis**

319 The synthesis of nanoparticles can be tuned by modifying several reaction parameters for jet-
320 mixing synthesis, the sodium borohydride concentration ($[\text{NaBH}_4]$) and the capping agent concentration
321 ($[\text{TSC}]$). From a commercial perspective, it is desirable to minimize the amounts of the different
322 components to reduce cost while still maintaining product quality. The reducing agent influences the
323 reaction rate. Excess reducing agents increase synthesis cost and may also contribute to higher ion
324 concentration in solution, causing eventual agglomeration of NPs.⁶⁵ To determine if an optimum
325 concentration for NaBH_4 exists to achieve monodisperse Ag NPs while limiting the reagent concentration
326 used, the standard jet-mixing synthesis is performed by varying the NaBH_4 concentrations between

327 0.03 mM, the stoichiometric amount⁴⁸ to 2.4 mM. The concentrations of AgNO₃ and TSC are maintained
328 at 0.2 mM each. It is observed that the FWHM narrows when using increasing concentrations of NaBH₄.
329 The most significant decrease in FWHM occurs for low NaBH₄ concentrations whereas the FWHM changes
330 less above a NaBH₄ concentration of 0.6 mM. This suggests that the standard concentration of NaBH₄ used
331 for this work (0.6 mM) is effective. A summary of the FWHMs calculated from the UV-vis spectra of all
332 runs for varying NaBH₄ concentration are reported in Table S6.

333 The second parameter investigated is the effect of capping agent concentration on NP synthesis.
334 The capping agent represents an important component to help stabilize nanoparticles in solution and prevent
335 agglomeration. An optimum capping agent concentration has also been previously reported for Ag NP batch
336 synthesis.¹⁹ In a synthesis in which TSC acts solely as the capping agent, it is shown that varying the
337 concentration of TSC from 0.05 mM to 1.5 mM results in agglomeration at low concentrations, coalescence
338 at high concentrations, and an intermediate concentration of the order of 0.1 mM results in NPs with a
339 narrow PSD. However, other works show a linear trend where the PSD is seen to increase or stay constant
340 with increase in the TSC concentration.⁶²

341 For the jet-mixing reactor, the effect is studied of TSC concentration on PSD of Ag NPs. The
342 standard jet-mixing Ag NP synthesis is performed using different concentrations of TSC, ranging from 1
343 μM to 0.8 mM. Each sample is analyzed by UV-vis, and the FWHM of the spectrum is calculated, as shown
344 in Figure 6. It is observed that the FWHM decreases as the concentration of TSC is increased from 0.001
345 mM to 0.05 mM and increases again as the TSC concentration is increased further. The summary of
346 FWHMs obtained for multiple jet-mixing runs conducted for different capping agent concentrations has
347 been listed in Table S7. Comparing this result to many different reported Ag NP
348 syntheses,^{10,13,16,23,25,26,28,31,32} the jet-mixing reactor is able to produce uniform Ag NPs with a low molar ratio
349 of capping agent to silver substrate, as shown in Figure 7. The concentration of capping agent that results
350 in the narrowest FWHM is 0.05 mM. This is less than the typical concentration used for typical batch
351 synthesis by a factor of four.

352 It is interesting to investigate how the batch synthesis performs at the optimum concentration
353 obtained for jet-mixing. A batch synthesis comparable to the jet-mixing synthesis at 0.05 mM TSC is carried
354 out and analyzed by UV-vis. The spectrum obtained for batch is compared against that for jet-mixing in
355 Figure 8. For the batch synthesis using 0.05 mM capping agent, the synthesis mixture has a UV-vis spectrum
356 is bi-modal, suggesting that insufficient TSC is present to prevent agglomeration. However, the jet-mixing
357 synthesis remains monomodal at 0.05 mM TSC. This observation is supported by representative TEM
358 images of batch and jet-mixing syntheses at 0.05 mM TSC, shown in Figure S9. From analyzing over 100
359 particles for each sample, the PSD is found to be 8 ± 5 nm for batch and 7 ± 2 nm for jet-mixing. This indicates
360 that mixing plays an important role in governing the effectiveness of the capping agent.

361 An interesting observation to note in Figure 6 is the increase in the polydispersity of the Ag NPs
362 synthesized at TSC concentrations above 0.05 mM, as indicated by the FWHM. It is hypothesized that this
363 is associated with an increase in the ion concentration of the solution. TSC is an anionic surfactant with
364 three carboxyl groups each bonded to a sodium ion. On dissolving in a polar solvent such as water, the
365 carboxylate salt in excess of that required for capping would dissociate into the sodium ions and the
366 carboxyl capping moiety. Any increase in the TSC concentration above 0.05 mM should hence lead to a
367 three-fold increase in the ion concentration in the solution, which has been known to cause agglomeration
368 for other systems.^{18,65} The effect of the ion concentration in the solution on PSD is investigated through a
369 series of experiments adding sodium nitrate (NaNO_3) to the reaction system. NaNO_3 is chosen as the salt
370 as the ions Na^+ and NO_3^- are already present in solution and will not react with other ions in solution, as
371 compared to ions such as Cl^- , which if added would cause precipitation of AgCl . Initially, the ion
372 concentration is increased prior to synthesis. NaNO_3 of equal concentration (32 mM) is added to each of the
373 standard synthesis solutions of NaBH_4 (0.6 mM) and AgNO_3 (0.2 mM) + TSC precursor solutions used for
374 standard synthesis. The concentration of TSC is varied from 0.003 to 0.2 mM. Jet-mixing runs at standard
375 main line and jet-line flowrates of 48 mL/h are performed for each TSC concentration. The Ag NP samples
376 produced are analyzed by UV-vis 15 minutes after collection, as shown in Figure S10. For the Ag NP
377 sample with 0.05 mM TSC, the FWHM calculated from the UV-vis spectrum comes out to be 58 nm,

378 greater than the FWHM achieved for a comparable jet-mixing run without any salt addition (i.e., 52 nm).
379 Similarly, for the Ag NP sample with 0.2 mM TSC, the FWHM calculated is 63 nm, significantly higher
380 than that achieved for a standard jet-mixing synthesis without NaNO_3 (57 nm). This observation suggests
381 the PSD is broadening.

382 This is also observed in Figure S11 showing Ag NP solutions prepared at TSC concentrations of
383 0.01 mM, 0.05 mM and 0.2 mM. The gray color of the Ag NP solution synthesized using 0.01 mM TSC
384 corroborates the aggregation of Ag and is presence of Ag in the form of bulk silver. The color of the solution
385 blue-shifts from gray to yellow on increasing the TSC concentration. The blue-shift demonstrates the
386 presence of smaller particles as the TSC concentration is increased.

387 While these results indicate that pre-synthetic addition of NaNO_3 to the Ag NP precursor solutions
388 promotes agglomeration of the synthesized Ag NPs, it is possible that addition of the salt before synthesis
389 can alter the kinetics of the reduction of AgNO_3 . Specifically, an increase in the NO_3^- and Na^+ ions in
390 solution may affect the rate of conversion of Ag^+ to Ag^0 , because of the common ion effect. To account for
391 this, the standard jet-mixing synthesis at 0.2 mM TSC is repeated, but with 32 mM NaNO_3 added post-
392 synthesis to the Ag NP solution. The resultant mixture is analyzed by UV-vis and TEM. The UV-vis
393 spectrum of the Ag NP sample before and after addition of 32 mM NaNO_3 is shown in Figure S12. It is
394 noticed that the spectrum broadens after addition of the salt, and the wavelength of maximum absorbance
395 red-shifts, indicating formation of larger particles. Further, the absorbance of the UV-vis spectrum drops
396 after salt addition, suggesting that the Ag NPs decrease in number, indicating increased aggregation. This
397 observation is corroborated by the TEM image of the sample in Figure S13 that show the presence of large
398 aggregates. To further validate our conclusion, these experiments were repeated for a higher concentration
399 (64 mM) of NaNO_3 . The results for these have also been shown in Figures S12 and S13 and confirm the
400 previous results for 32 mM NaNO_3 . These experiments demonstrate that an increase in the ion concentration
401 of the Ag NP solution caused by the addition of excess TSC could indeed increase the sample
402 polydispersity. Hence, limiting the TSC concentration used in synthesis is not only beneficial in reducing
403 the cost of synthesis but also producing NPs with a more monodisperse PSD.

404 **3.5. Stability of Ag NPs synthesized by Batch and Jet-mixing at optimum TSC concentration**

405 An important consideration for the synthesis of Ag NPs is stability. While it is desirable to reduce
406 the amount of capping agent used, the resultant nanoparticles should also be stable in solution. To analyze
407 nanoparticle stability, the batch and JM solutions synthesized with 0.05 mM TSC at otherwise standard
408 conditions are monitored over a long-term period. Each solution is divided into two separate samples post-
409 synthesis to check similarity in growth profiles between identical samples. Further, two separate syntheses
410 for batch and JM each are also performed for reproducibility. Equal volumes of each sample are stored in
411 the refrigerator at 4°C to prevent TSC degradation. The samples are evenly covered with aluminum foil to
412 keep out external light. The FWHM of the samples is monitored via UV-vis at fixed intervals, starting from
413 15 minutes up to 1 month after synthesis. The FWHMs obtained for both batch and JM samples at each
414 time of analysis are plotted in Figure 9. Values for FWHM for batch and JM-synthesized samples have
415 been listed in Table S8 and Table S9, respectively. While the FWHM for both batch and jet-mixing increase
416 with time, the batch synthesized sample starts out with a broad FWHM as compared to the jet-mixing
417 synthesized sample and remains so throughout the period of monitoring. The FWHM of the JM-synthesized
418 sample, after 1 month, is 18 nm smaller than the batch-synthesized sample. These results suggest that JM-
419 synthesized samples at 0.05 mM TSC tend to remain monodisperse even on long storage.

420

421 **4. Summary**

422 A jet-mixing reactor is used to synthesize Ag NPs that are monodisperse (5 ± 2 nm) with a narrow
423 SPR spectrum. It is viable to produce Ag NP in large quantities by increasing reactor run-time, because of
424 the consistent product quality produced and reproducible synthesis, as indicated by UV-vis. On varying the
425 concentration of capping agent TSC in the jet-mixing synthesis, it is found that there is an optimum
426 concentration of TSC (0.05 mM). At this optimum concentration, a monodisperse PSD is observed as
427 suggested by a minimum SPR FWHM and corroborated using TEM images. This concentration of capping
428 agent is lower by a factor of four than other reports while maintaining high quality particles. This optimum
429 concentration provides balanced stabilization necessary to prevent agglomeration while maintaining a low

430 solution ion concentration. It is shown that concentration higher than optimum results in destabilization of
431 the solution by an increase in the ion concentration causing Ag NP aggregation. External addition of NaNO_3
432 to the product solution also produces the same effect, confirming the hypothesis. With the lower
433 concentration of capping agent of 0.05 mM, the nanoparticles produced using the jet-mixing reactor retain
434 a narrower FWHM than the nanoparticles produced in the batch process. Overall, the jet-mixing reactor
435 provides an efficient way to produce monodisperse particles in a continuous manner.

436

437 5. Acknowledgements

438 The authors would like to acknowledge funding from the National Science Foundation (CBET
439 1653587) and The Ohio State University Institute of Materials Research (EMR-G00018 and IMR-FG0211).
440 Images presented in this report were generated using the instruments and services at the Campus
441 Microscopy and Imaging Facility, The Ohio State University. This facility is supported in part by grant P30
442 CA016058, National Cancer Institute, Bethesda, MD. The authors would also like to acknowledge Mariah
443 Whitaker, Abhilasha Dehankar, and Kilho Lee for useful discussions.

444

445 6. Notation

446 Q_r = solution flowrate in the main line.

447 Q_j = the solution flowrate in the jet line.

448 $[A]$ = Molar concentration of species A in solution.

449

450 6. References

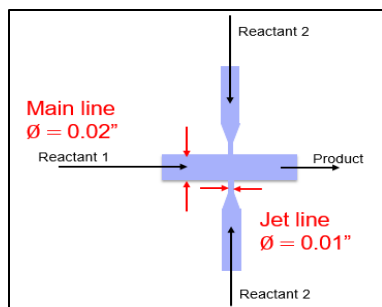
- 451 1 X. Wu, P. L. Redmond, H. Liu, Y. Chen, M. Steigerwald and L. Brus, *J. Am. Chem. Soc.*, 2008,
452 **130**, 9500–9506.
- 453 2 R. L. Hartman, J. P. McMullen and K. F. Jensen, *Angew. Chem. Int. Ed.*, 2011, **50**, 7502–19.
- 454 3 N. T. K. Thanh, N. Maclean and S. Mahiddine, *Chem. Rev.*, 2014, **114**, 7610–7630.
- 455 4 R. Bakhtiar, *J. Chem. Educ.*, 2013, **90**, 203–209.

- 456 5 C. A. Dos Santos, M. M. Seckler, A. P. Ingle, I. Gupta, S. Galdiero, M. Galdiero, A. Gade and M.
457 Rai, *J. Pharm. Sci.*, 2014, **103**, 1931–1944.
- 458 6 N. L. Pacioni, C. D. Borsarelli, V. Rey and A. V Veglia, *Silver Nanoparticle Applications*, 2015.
459 7 D. Denkova, *Optical characterization of plasmonic nanostructures : near-field imaging of the
460 magnetic field of light*, 2014, vol. 3168.
- 461 8 E. Petryayeva and U. J. Krull, *Anal. Chim. Acta*, 2011, **706**, 8–24.
- 462 9 B. Calderon-Jimenez, G. F. Sarmanho, K. E. Murphy, A. R. Montoro and J. R. Vega-Baudrit, *J.
463 Res. Natl. Inst. Stand. Technol.*, 2017, **122**, 1–10.
- 464 10 S. Agnihotri, S. Mukherji and S. Mukherji, *RSC Adv.*, 2014, **4**, 3974–3983.
- 465 11 M. S. Saleh, C. Hu and R. Panat, *Sci. Adv.*, 2017, **3**, e1601986.
- 466 12 L. M. Molina, S. Lee, K. Sell, G. Barcaro, A. Fortunelli, B. Lee, S. Seifert, R. E. Winans, J. W.
467 Elam, M. J. Pellin, I. Barke, V. Von Oeynhausen, Y. Lei, R. J. Meyer, J. A. Alonso, A. Fraile, A.
468 Kleibert, S. Giorgio, C. R. Henry, K. Meiwes-broer and S. Vajda, *Catal. Today*, 2011, **160**, 116–
469 130.
- 470 13 C. Petit, P. Lixon and M. P. Pileni, *J. Phys. Chem.*, 1993, **97**, 12974–12983.
- 471 14 B. Ajitha, Y. A. Kumar Reddy, P. S. Reddy, H.-J. Jeon and C. W. Ahn, *RSC Adv.*, 2016, **6**, 36171–
472 36179.
- 473 15 H. Fathi, J. P. Kelly, V. R. Vasquez and O. A. Graeve, *Langmuir*, 2012, **28**, 9267–9274.
- 474 16 D. Singha, N. Barman and K. Sahu, *J. Colloid Interface Sci.*, 2014, **413**, 37–42.
- 475 17 J. D. Martin, L. Telgmann and C. D. Metcalfe, *Bull. Environ. Contam. Toxicol.*, 2017, **98**, 589–
476 594.
- 477 18 R. A. French, A. R. Jacobson, B. Kim, S. L. Isley and R. L. E. E. Penn, *Environ. Sci. Technol.*,
478 2009, **43**, 1354–1359.
- 479 19 A. Henglein and M. Giersig, *J. Phys. Chem. B*, 1999, **103**, 9533–9539.
- 480 20 R. Southey, *The Story of the Three Bears*, Longman, Rees, etc., 1837.
- 481 21 S. Silvestrini, T. Carofiglio and M. Maggini, *Chem. Commun.*, 2013, **49**, 84–86.

- 482 22 Z. Niu and Y. Li, *Chem. Mater.*, 2014, **26**, 72–83.
- 483 23 M. Carboni, L. Capretto, D. Carugo, E. Stulz and X. Zhang, *J. Mater. Chem. C*, 2013, **1**, 7540.
- 484 24 X. Dong, X. Ji, H. Wu, L. Zhao, J. Li and W. Yang, *J. Phys. Chem. C*, 2009, **113**, 6573–6576.
- 485 25 J. Liu, P. Raveendran, Z. Shervani, Y. Ikushima and Y. Hakuta, *Chem. - A Eur. J.*, 2005, **11**,
486 1854–1860.
- 487 26 A. Taleb, C. Petit and M. P. Pileni, *Chem. Mater.*, 1997, **9**, 950–959.
- 488 27 C. Petit, P. Lixon and M. P. Pileni, *J. Phys. Chem.*, 1993, **97**, 12974–12983.
- 489 28 X. Z. Lin, A. D. Terepka and H. Yang, *Nano Lett.*, 2004, **4**, 2227–2232.
- 490 29 D. Paramelle, A. Sadovoy, S. Gorelik, P. Free, J. Hobley and D. G. Fernig, *Analyst*, 2014, **139**,
491 4855.
- 492 30 T. C. Prathna, N. Chandrasekaran, A. M. Raichur and A. Mukherjee, *Colloids Surfaces B*
493 *Biointerfaces*, 2011, **82**, 152–159.
- 494 31 B. Pietrobon and V. Kitaev, *Chem. Mater.*, 2008, **20**, 5186–5190.
- 495 32 S. T. He, Y. L. Liu and H. Maeda, *J. Nanoparticle Res.*, 2008, **10**, 209–215.
- 496 33 S. Iravani, H. Korbekandi, S. V. Mirmohammadi and B. Zolfaghari, *Res. Pharm. Sci.*, 2014, **9**,
497 385–406.
- 498 34 K. Sen Chou, Y. C. Chang and L. H. Chiu, *Ind. Eng. Chem. Res.*, 2012, **51**, 4905–4910.
- 499 35 W. Zhang, X. Qiao, Q. Chen, Y. Cai and H. Chen, *Appl. Surf. Sci.*, 2012, **258**, 5909–5913.
- 500 36 M. Wuithschick, B. Paul, R. Bienert, A. Sarfraz, U. Vainio, M. Sztucki, R. Kraehnert, P. Strasser,
501 K. Rademann, F. Emmerling and J. Polte, *Chem. Mater.*, 2013, **25**, 4679–4689.
- 502 37 L. Xu, J. Peng, M. Yan, D. Zhang and A. Q. Shen, *Chem. Eng. Process. Process Intensif.*, 2016,
503 **102**, 186–193.
- 504 38 J. Polte, X. Tuaeov, M. Wuithschick, A. Fischer, A. F. Thuenemann, K. Rademann, R. Kraehnert
505 and F. Emmerling, *ACS Nano*, 2012, **6**, 5791–5802.
- 506 39 S. Mülhopt, S. Diabaté, M. Dilger, C. Adelhelm, C. Anderlohr, T. Bergfeldt, J. Gómez de la Torre,
507 Y. Jiang, E. Valsami-Jones, D. Langevin, I. Lynch, E. Mahon, I. Nelissen, J. Piella, V. Puentes, S.

- 508 Ray, R. Schneider, T. Wilkins, C. Weiss and H.-R. Paur, *Nanomaterials*, 2018, **8**, 311.
- 509 40 L. Mockus, J. J. Peterson, J. M. Lainez and G. V. Reklaitis, *Org. Proc. Res. Dev.*, 2015, **19**, 908–
510 914.
- 511 41 B. K. Johnson and R. K. Prud'homme, *AIChE J.*, 2003, **49**, 2264–2282.
- 512 42 M. M. Alvarez, J. M. Zalc, T. Shinbrot, P. E. Arratia and F. J. Muzzio, *AIChE J.*, 2002, **48**, 2135–
513 2148.
- 514 43 Brian K Johnson and R. K. Prud'homme, *Aust. J. Chem.*, 2003, 1021–1024.
- 515 44 R. L. Hartman and K. F. Jensen, *Lab Chip*, 2009, **9**, 2495.
- 516 45 S. Marre and K. F. Jensen, *Chem. Soc. Rev.*, 2010, **39**, 1183–202.
- 517 46 J. M. Ottino, *Phys. Fluids*, 2010, **22**, 1–12.
- 518 47 X. Z. Lin, X. Teng and H. Yang, *Langmuir*, 2003, **19**, 10081–10085.
- 519 48 R. Baber, L. Mazzei, T. K. Thanh and A. Gavriilidis, *RSC Adv.*, 2015, **5**, 95585–95591.
- 520 49 R. Baber, L. Mazzei, N. T. K. Thanh and A. Gavriilidis, *Nanoscale*, 2017, 14149–14161.
- 521 50 D. V. R. Kumar, M. Kasture, A. A. Prabhune, C. V. Ramana, B. L. V. Prasad and A. A. Kulkarni,
522 *Green Chem.*, 2010, **12**, 609.
- 523 51 K. S. Iyer, C. L. Raston and M. Saunders, *Lab Chip*, 2007, **7**, 1800.
- 524 52 H. Mehenni, L. Sinatra, R. Mahfouz, K. Katsiev and O. M. Bakr, *RSC Adv.*, 2013, **3**, 22397.
- 525 53 J. Boleininger, A. Kurz, V. Reuss and C. So, *Phys. Chem. Chem. Phys.*, 2006, **8**, 3824–3827.
- 526 54 K. J. Hartlieb, M. Saunders, R. J. J. Jachuck and C. L. Raston, *Green Chem.*, 2010, **12**, 1012.
- 527 55 D. Mitrakos, J. Jokiniemi, U. Backman and C. Housiadas, *J. Nanoparticle Res.*, 2008, **10**, 153–
528 161.
- 529 56 A. Günther, S. A. Khan, M. Thalmann, F. Trachsel and K. F. Jensen, *Lab Chip*, 2004, **4**, 278–286.
- 530 57 A. Parulkar and N. A. Brunelli, *Ind. Eng. Chem. Res.*, 2017, **56**, 10384–10392.
- 531 58 D. M. Holunga, R. C. Flagan and H. A. Atwater, *Ind. Eng. Chem. Res.*, 2005, **44**, 6332–6341.
- 532 59 G. N. Glavee, K. J. Klabunde, C. M. Sorensen and G. C. Hadjapanayis, *Langmuir*, 1992, **8**, 771–
533 773.

- 534 60 K.-J. Wu, G. M. De Varine Bohan and L. Torrente-Murciano, *React. Chem. Eng.*, 2017, **2**, 116–
535 128.
- 536 61 C. A. Schneider, W. S. Rasband and K. W. Eliceiri, *Nat. Methods*, 2012, **9**, 671–675.
- 537 62 G. A. Patil, M. L. Bari, B. A. Bhanvase, V. Ganvir, S. Mishra and S. H. Sonawane, *Chem. Eng.*
538 *Process. Process Intensif.*, 2012, **62**, 69–77.
- 539 63 S. D. Solomon, M. Bahadory, A. V Jeyarajasingam, S. A. Rutkowsky, C. Boritz and L. Mulfinger,
540 *J. Chem. Educ.*, 2007, **84**, 322–325.
- 541 64 R. Baber, L. Mazzei, N. T. K. Thanh and A. Gavriilidis, *J. Flow Chem.*, 2016, **6**, 268–278.
- 542 65 J. F. A. de Oliveira and M. B. Cardoso, *Langmuir*, 2014, **30**, 4879–4886.
- 543
- 544

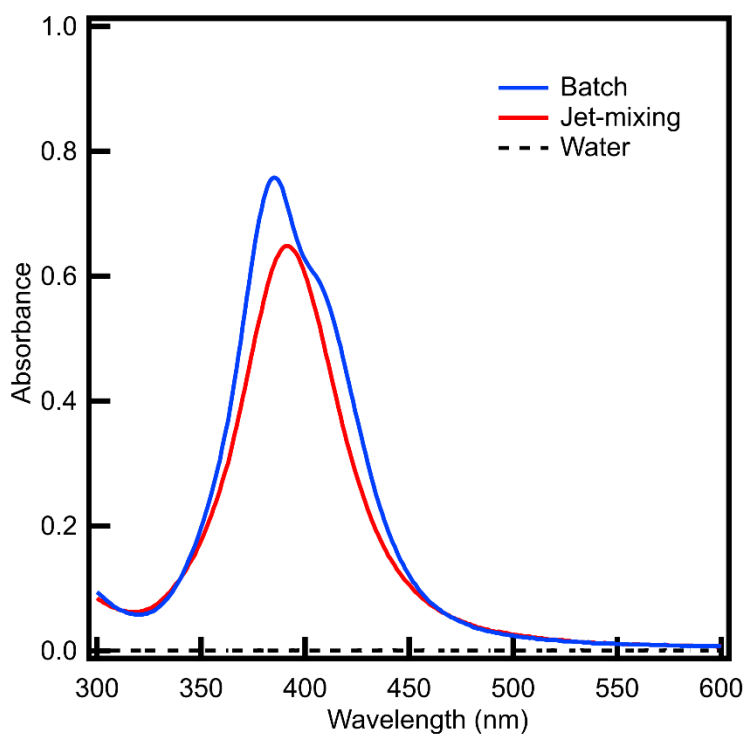


545

546 **Figure 1.** The reactor design showing the main line ($d_r = 0.04''$) carrying reactant 1 and orthogonal jet lines

547 ($d_j = 0.02''$) carrying reactant 2. The product is collected downstream of the reactor.

548



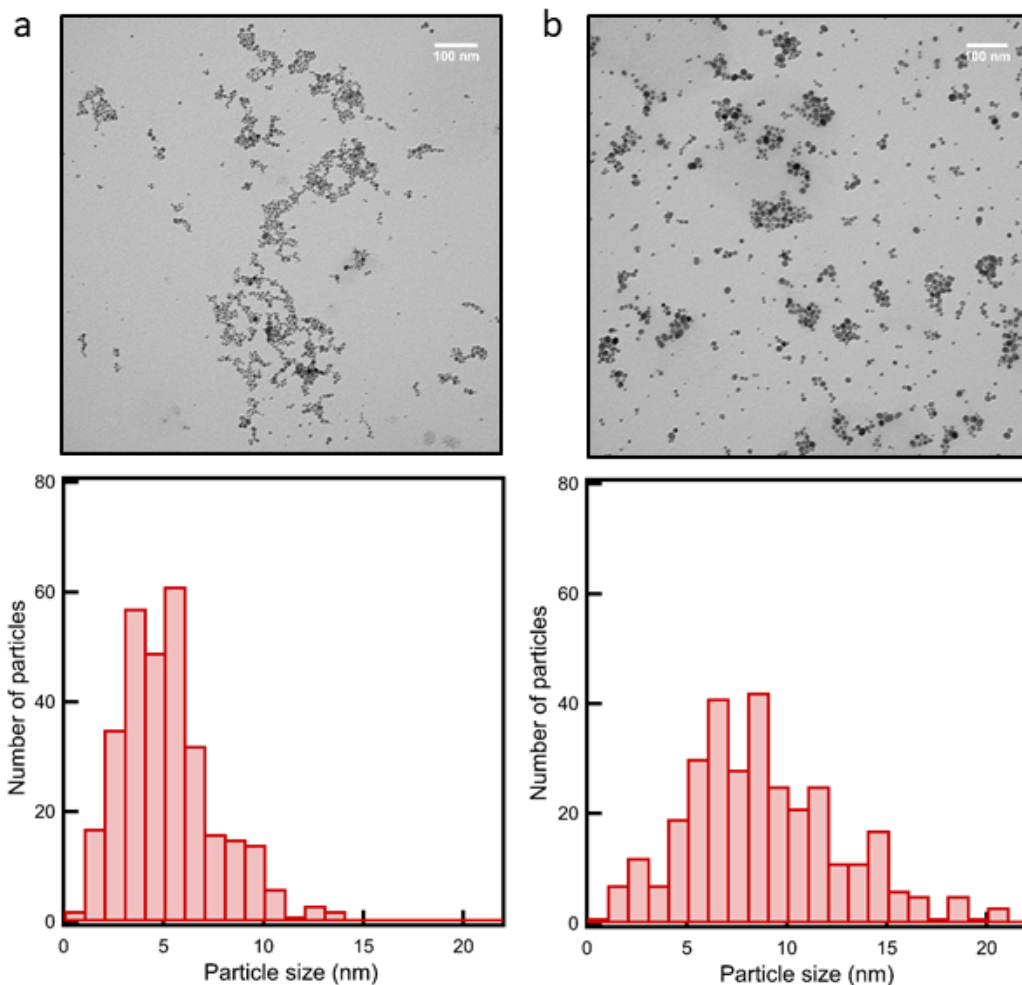
549

550 **Figure 2.** UV-vis spectra of Ag NPs synthesized by standard batch (*blue*) and jet-mixing (*red*) synthesis.

551 Synthesis conditions are as follows: $Q_r = Q_j = 48$ mL/h for jet-mixing; $[\text{NaBH}_4] = 0.6$ mM, $[\text{AgNO}_3] =$

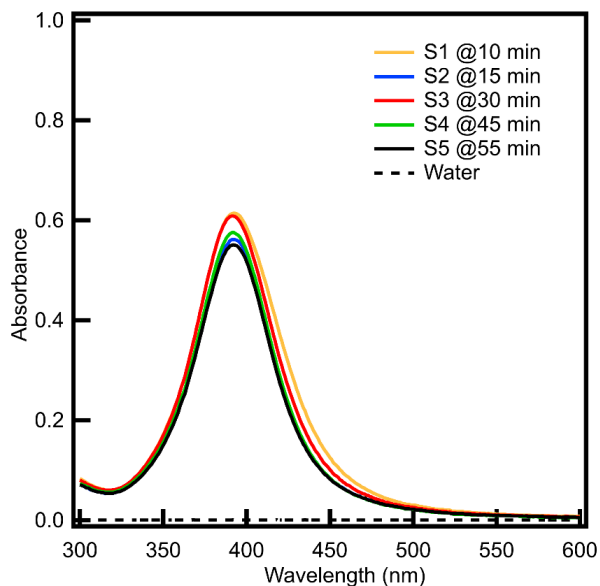
552 0.2 mM, $[\text{TSC}] = 0.2$ mM for both syntheses.

553



554

555 **Figure 3.** TEM images and corresponding PSDs of standard (a) jet-mixing (5 ± 2 nm) and (b) batch (9 ± 4
556 nm) syntheses. The distributions are calculated by the size analysis of 300 particles for each synthesis, using
557 ImageJ software. Synthesis conditions are as follows: $Q_r = Q_j = 48$ mL/h for jet-mixing; $[\text{NaBH}_4] = 0.6$
558 mM, $[\text{AgNO}_3] = 0.2$ mM, $[\text{TSC}] = 0.2$ mM for both syntheses.

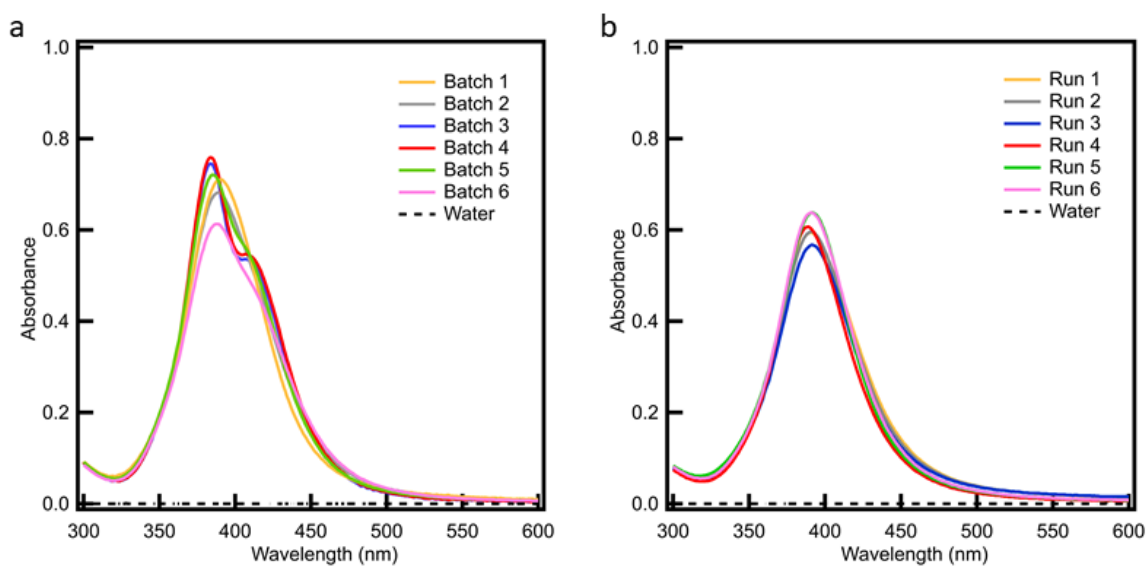


559

560 **Figure 4.** UV-vis spectra of Ag NP samples collected at various times during a standard jet-mixing run.

561 The legend Sn @t min indicates the nth sample collected at time t min after starting run. Synthesis

562 conditions are as follows: $Q_r = Q_j = 48$ mL/h; $[\text{NaBH}_4] = 0.6$ mM, $[\text{AgNO}_3] = 0.2$ mM, $[\text{TSC}] = 0.2$ mM.



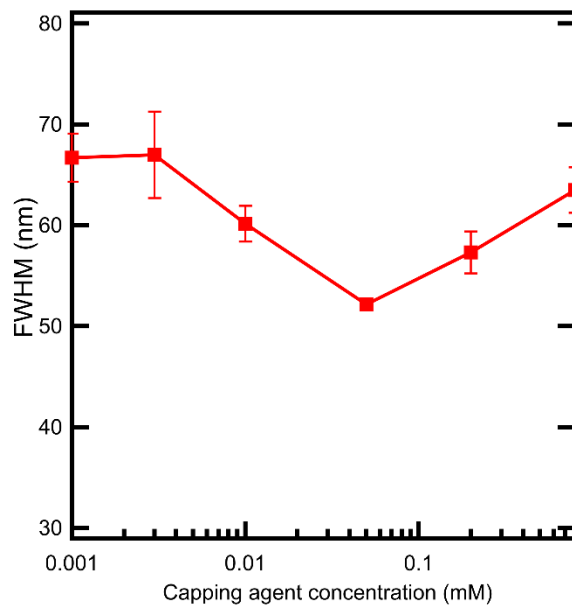
563

564 **Figure 5.** UV-vis spectra of six separate runs of Ag NP synthesis in a standard (a) batch synthesis in a 250

565 mL round bottom flask at 200 RPM; (b) jet-mixing synthesis with NaBH_4 solution flowing through the

566 main line at 48 mL/h and $\text{AgNO}_3 + \text{TSC}$ solution flowing through the jet line at 48 mL/h. Synthesis

567 conditions are as follows: $[\text{NaBH}_4] = 0.6$ mM, $[\text{AgNO}_3] = 0.2$ mM, $[\text{TSC}] = 0.2$ mM for both syntheses.



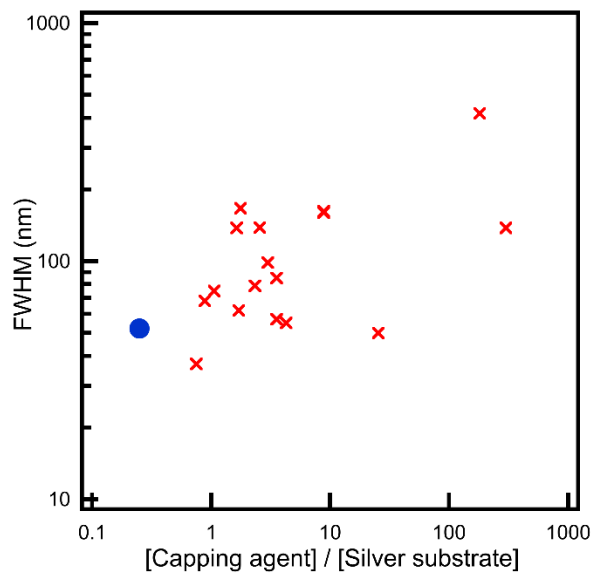
568

569 **Figure 6.** Comparison of FWHM of Ag NPs synthesized via jet-mixing, calculated from UV-vis spectra,

570 against the TSC concentration (mM) used in the run. The TSC concentration is varied while keeping other

571 synthesis conditions at the following values: $Q_r = Q_j = 48$ mL/h; $[\text{NaBH}_4] = 0.6$ mM, $[\text{AgNO}_3] = 0.2$ mM.

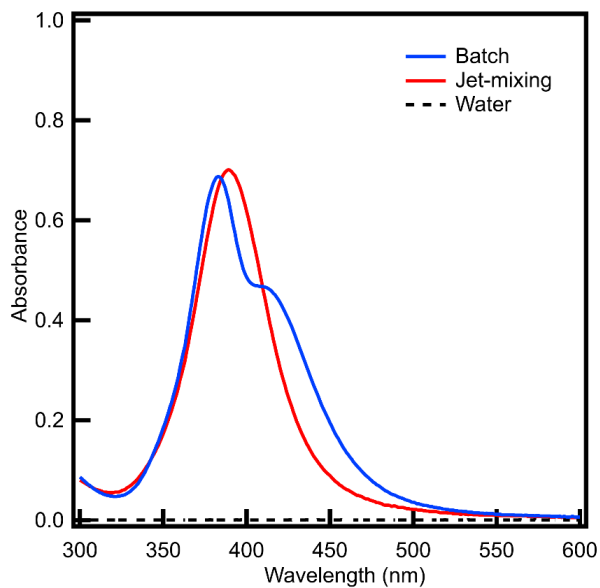
572



573

574 **Figure 7.** Plot summarizing the FWHM of Ag NPs, obtained for different molar ratios of capping agent to
575 silver substrate. The data includes a number of studies from literature (*red*) and the data obtained in this
576 work (*blue*). Jet-mixing synthesis results in a narrow FWHM of 55 nm while requiring a low capping agent
577 concentration of 0.05 mM. Other synthesis conditions are as follows: $Q_r = Q_j = 48$ mL/h; $[\text{NaBH}_4] = 0.6$
578 mM, $[\text{AgNO}_3] = 0.2$ mM. The capping agent to silver substrate molar ratios have been calculated based on
579 parameters such as % vol., weight, or molar concentration of the Ag NP precursors reported in previous
580 works.^{10,13,16,23,25,26,28,31,32}

581

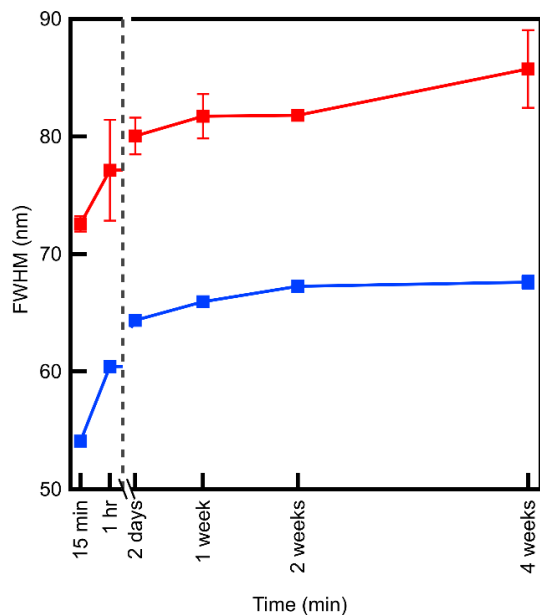


582

583 **Figure 8.** UV-vis spectra comparing batch (*blue*) and jet-mixing (*red*) syntheses at 0.05 mM TSC; the
584 optimum concentration obtained for jet-mixing. Other synthesis conditions are as follows: $Q_r = Q_j =$
585 48 mL/h for jet-mixing; $[\text{NaBH}_4] = 0.6$ mM, $[\text{AgNO}_3] = 0.2$ mM for both syntheses.

586

587



588

589 **Figure 9.** FWHM obtained via UV-Vis for standard Ag NP batch and jet-mixing syntheses with 0.05 mM

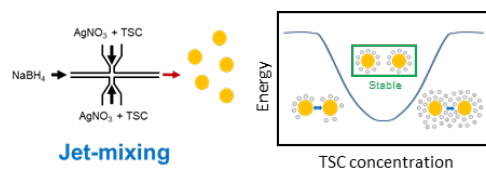
590 TSC, plotted against different times of analysis post-synthesis from 15 minutes to 1 month. Other

591 synthesis conditions are as follows: $Q_r = Q_j = 48$ mL/h for jet-mixing; $[\text{NaBH}_4] = 0.6$ mM, $[\text{AgNO}_3] =$

592 0.2 mM for both syntheses.

593

594 Graphical Abstract



595

596 The jet-mixing reactor can continuously produce monodisperse silver nanoparticles using limited amounts
597 of capping agent.

598